PCCP

PAPER

View Article Online
View Journal | View Issue

Cite this: *Phys. Chem. Chem. Phys.*, 2016, **18**, 14191

Tuning the electronic and mechanical properties of penta-graphene *via* hydrogenation and fluorination

Xiaoyin Li,[ab] Shunhong Zhang,[ab] Fancy Qian Wang,[ab] Yaguang Guo,[a] Jie Liu[a] and Qian Wang*[ab]

Received 17th February 2016,
Accepted 30th March 2016

DOI: 10.1039/c6cp01092j

www.rsc.org/pccp

Penta-graphene has recently been proposed as a new allotrope of carbon composed of pure pentagons, and displays many novel properties going beyond graphene [Zhang *et al.*, *Proc. Natl. Acad. Sci. U. S. A.*, 2015, **112**, 2372]. To further explore the property modulations, we have carried out a theoretical investigation of the hydrogenated and fluorinated penta-graphene sheets. Our first-principles calculations reveal that hydrogenation and fluorination can effectively tune the electronic and mechanical properties of penta-graphene: turning the sheet from semiconducting to insulating; changing the Poisson's ratio from negative to positive, and reducing the Young's modulus. Moreover, the band gaps of the hydrogenated and fluorinated penta-graphene sheets are larger than those of fully hydrogenated and fluorinated graphene by 0.37 and 0.04 eV, respectively. The phonon dispersions and *ab initio* molecular dynamics simulations confirm that the surface modified penta-graphene sheets are dynamically and thermally stable, and show that the hydrogenated penta-graphene has more Raman-active modes with higher frequencies as compared to the fluorinated penta-graphene.

Introduction

Currently, two-dimensional (2D) atomic-layer-based materials are being widely studied due to their unique electronic and magnetic properties. One such example is that of graphene,[1] which has a covalently bonded honeycomb lattice exhibiting robust stability and exceptional properties such as high carrier mobility, thermal conductivity, optical transmittance and anomalous quantum Hall effect.[2,3] However, graphene is a zero band-gap semimetal, limiting its possible application in the field of optics, optoelectronics and microelectronics. Thus a wealth of 2D carbon allotropes beyond graphene and their derivatives have since been hotly pursued.[4–7] For instance, recently a new three-fold and four-fold coordinated hybrid carbon sheet composed of only pentagons, penta-graphene, was proposed.[4] It is a quasi-direct band gap semiconductor with a band gap of 3.25 eV and exhibits exceptional mechanical properties such as negative Poisson's ratio and ultrahigh ideal strength under biaxial strain, making it a versatile material for many promising applications. On the other hand, functionalization of graphene for opening its band gap[8] and tuning its properties for more fascinating applications has received considerable attention.[9] First-principles calculations have demonstrated that surface modification can effectively tune the electronic, magnetic and mechanical properties of graphene, going from metallic to semiconducting,[10] and from nonmagnetic to magnetic.[11,12] Thus, a question arises: how do the properties of penta-graphene change upon surface modification?

In this work, we have studied the chemical functionalization of penta-graphene by introducing hydrogen and fluorine atoms on both sides of this sheet, respectively. We have calculated the adsorption energy, phonon dispersion and thermal stability, and electronic and mechanical properties of the hydrogenated and fluorinated penta-graphene sheets. We show that both hydrogenated and fluorinated penta-graphene sheets are stable, and their electronic band structures and elastic moduli differ from those of pristine penta-graphene.

Methods

Our first-principles calculations and *ab initio* molecular dynamics (AIMD) simulations are based on density functional theory and all of the calculations are performed using the Vienna *Ab initio* Simulation Package (VASP).[13] A vacuum space of 20 Å in the direction perpendicular to the sheet is used to separate it from its periodic images. Wave functions are

[a] *Center for Applied Physics and Technology, College of Engineering, Peking University, Beijing 100871, China. E-mail: qianwang2@pku.edu.cn*
[b] *Key Laboratory of High Energy Density Physics Simulations, Ministry of Education, Beijing 100871, China*

expanded using the projector augmented wave (PAW) method with a kinetic energy cutoff of 500 eV. The exchange–correlation potential is incorporated using the generalized gradient approximation (GGA). The Perdew–Burke–Ernzerhof (PBE)[14] functional is used in most of our calculations whereas the hybrid Heyd–Scuseria–Ernzerhof (HSE06)[15,16] functional is used for high-accuracy electronic structure calculations. The first Brillouin zone is represented by k points in the reciprocal space sampled using the Monkhorst–Pack scheme[17] with a grid density of $2\pi \times 0.02$ Å^{-1}. The lattice and atoms are relaxed without any symmetry constraints. The convergence criterion of total energy is set as 1 meV in AIMD simulations and temperature control is achieved using the Nosé thermostat.[18] Phonon calculations are performed by using the finite displacement method implemented in the phonopy package.[19] For geometry optimization, the convergence thresholds for total energy and force components are set as 10^{-4} eV and 0.01 eV Å^{-1}, respectively.

Results and discussion

Unlike graphene where all carbon atoms are sp^2-hybridized, there are two chemically nonequivalent carbon atoms in penta-graphene. The unit cell contains two four-fold coordinated and four three-fold coordinated carbon atoms. Due to the special atomic configuration, we found that only the three-fold coordinated carbon atoms can adsorb hydrogen or fluorine atoms forming the quasi-2D hydrogenated or fluorinated penta-graphene sheets, as shown in Fig. 1, where all carbon atoms become four-fold coordinated. In these two structures, the ratio of C : H or C : F is 3 : 2, differing from that of 1 : 1 in the fully hydrogenated (graphane)[20] or fluorinated graphene (fluorographene).[12] After full geometry optimization, we found that the two functionalized structures still retain the $P\bar{4}2_1m$ symmetry, indicating that the full hydrogenation/fluorination does not change the crystallographic symmetry of penta-graphene. For convenience of discussion, we group the four-fold and three-fold coordinated carbon atoms of the pristine penta-graphene as C1 and C2, respectively, and label the hydrogenated/fluorinated penta-graphene as H-PG-H/F-PG-F. Accordingly, the hydrogenated/fluorinated graphene is labeled as H-G-H/F-G-F for comparison. The bond lengths of C1–C2 and C2–C2 are 1.55/1.57 Å and 1.55/1.58 Å for the hydrogenated/fluorinated penta-graphene, respectively, which are close to that of 1.53 Å in diamond, but longer than that of 1.42 Å in graphene, showing a single bond character. The bond angles $\theta_{C2-C1-C2}$ and $\theta_{C1-C2-C1}$ are 116.9°/117.8° and 105.9°/106.7°, respectively, indicating the distorted sp^3 hybridization of the carbon atoms. The increase of the C2–C2 bond length from 1.34 Å to 1.55/1.58 Å due to the hydrogenation/fluorination implies the transformation from the double bond to the single bond, while the change of the C1–C2 bond length is subtle after hydrogenation or fluorination. The optimized structure parameters of H-PG-H and F-PG-F as well as H-G-H and F-G-F are summarized in Table 1. We define the buckling height Δ as the vertical coordinate difference of the top and bottom carbon layers (see Fig. 1). One can see that after hydrogenation/fluorination, the buckling height increases to 1.62/1.60 Å from 1.20 Å of the pristine penta-graphene, while for the hydrogenated/fluorinated graphene, Δ is 0.46/0.49 Å respectively.

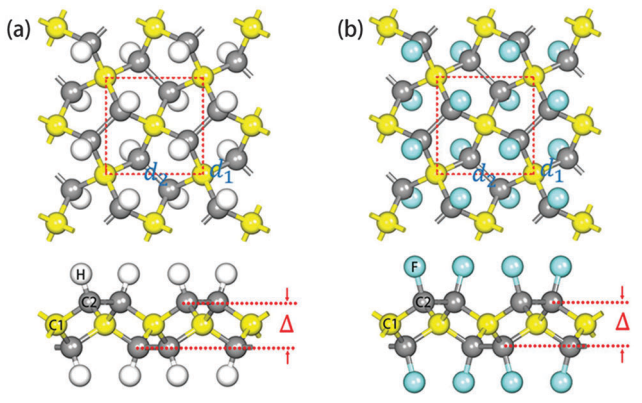

Fig. 1 Top and side views of the optimized structures of (a) the hydrogenated and (b) fluorinated penta-graphene. The squares marked by red dashed lines denote the unit cells, and the highlighted yellow spheres represent the four-fold coordinated C atoms in the pristine penta-graphene.

Table 1 Optimized structure parameters, distance Δ between the top and bottom layers of the carbon atoms, electronic band gap E_g calculated by using the PBE/HSE06 functional, and binding energy E_b of the functionalized penta-graphene and graphene

	H-PG-H	F-PG-F	H-G-H	F-G-F
d (C1–C2) (Å)	1.55	1.57	—	—
d (C2–C2) (Å)	1.55	1.58	1.53	1.58
d (C–H/C–F) (Å)	1.10	1.37	1.11	1.38
$\theta_{C2-C1-C2}/\theta_{C1-C2-C1}$	116.9/105.9°	117.8/106.7°	—	—
Δ (Å)	1.62	1.60	0.46	0.49
E_g (PBE) (eV)	4.29	3.36	3.86	3.11
E_g (HSE06) (eV)	5.35	4.78	4.97	4.74
E_b (eV per atom)	3.65	4.22	2.47	2.92

We then calculated the binding energy of the hydrogen/fluorine atom with penta-graphene, which is defined by $E_b = -(E_{total} - E_{PG} - 4E_{adatom})/4$, where E_{total}, E_{PG}, and E_{adatom} stand for, respectively, the total energy of the ground state configuration of the hydrogenated/fluorinated penta-graphene, pristine penta-graphene, and isolated hydrogen/fluorine atom. There are four adsorbed hydrogen/fluorine atoms per unit cell, and the binding energy is averaged on each adsorbed atom. The calculated binding energy is 3.65 eV/H and 4.22 eV/F for the hydrogenated and fluorinated penta-graphene, respectively. The large binding energy indicates that the attractive interactions between hydrogen/fluorine atoms and the penta-graphene sheet are strong. The possible reason is that the adsorption of hydrogen/fluorine atoms on penta-graphene enlarges the C–C bond length due to the formation of C–H/C–F bonds and thus partially releases the stress imposed by the pentagonal configuration. This is reminiscent of the experimentally synthesized dodecahedral C_{20} fullerene, which was obtained by using hydrogenated or brominated C_{20} as the precursor.[21,22] For comparison, we also calculated the binding energy of hydrogen/fluorine atoms with graphene, which is 2.47 eV/H and 2.92 eV/F, respectively, in good agreement with previous calculations.[23,24] The larger binding

energy of hydrogen/fluorine atoms with penta-graphene indicates that the adsorption of hydrogen/fluorine is energetically favorable over that of graphene. This can be understood from the following facts: the buckling structure of penta-graphene has more space for the adsorbed atoms, and the three-fold coordinated C2 atoms in penta-graphene are chemically more active than the C atoms in graphene that are relatively inert due to the delocalized π electrons. In addition, the surface modification of penta-graphene elongates the bond length of C2–C2, thus partially releasing the strain stored in the pristine structure while for graphene, the structure becomes distorted after the surface modification, which introduces strain reversely.

To examine the stability of the hydrogenated/fluorinated penta-graphene, we first performed *ab initio* molecular dynamics simulations at 300 K and 1000 K, respectively, for 10 000 steps with a time step of 1 fs. To reduce the periodic constraints, the 2D sheet of the hydrogenated/fluorinated penta-graphene is simulated using a (4 × 4) supercell containing 160 atoms. The fluctuations of the total potential energies and the geometric structures at the end of the AIMD simulations for the hydrogenated/fluorinated penta-graphene are presented in Fig. 2, which show in both cases of the hydrogenated and fluorinated penta-graphene that the average values of the total potential energies remain nearly constant and the 2D sheets maintain their integrated structures during the molecular dynamics simulations at 300 K and 1000 K, respectively, indicating that both the hydrogenated and fluorinated penta-graphene sheets are not only thermally stable at room temperature, but can also withstand temperatures as high as 1000 K.

We then calculated the phonon dispersions of the hydrogenated and fluorinated penta-graphene sheets along the high symmetric paths in the first Brillouin zone to study their dynamic stability. The results are presented in Fig. 3. No imaginary frequencies are observed in the entire Brillouin zone for both of the two structures, confirming the dynamical stability of the hydrogenated/fluorinated penta-graphene. Similar to the case of graphene[25,26] and penta-graphene, the phonon spectra of H-PG-H and F-PG-F both exist in three distinct acoustic modes and the two-fold degeneracy remains on the X–M path, which is the boundary of the first Brillouin zone. One can see from Fig. 3(a_1) and (b) that a large phonon gap is observed in the case of H-PG-H, while for F-PG-F the phonon gap is relatively small. After a careful analysis of the corresponding atom-resolved phonon density of states (PhDOS), we found that, for H-PG-H, the σ bond between H and C2 atoms plays a dominant role in the dispersionless high-frequency modes, which agrees with that of the previous reported hydrocarbon structures.[27,28] However, the formation of a single bond between F and C2 atoms in F-PG-F only leads to the dense phonon modes in the range of 0–10 THz, which can be seen when comparing (a_2) and (b) in Fig. 3, thus resulting in a relatively smaller phonon gap. We argue that the different phonon dispersion relations between the hydrogenated and fluorinated penta-graphene can be partially attributed to the differences in electronegativity and atomic mass between hydrogen and fluorine atoms. The surface modification breaks the double bonds between the C2 atoms, which results in the absence of high-frequency modes in the range of 45–50 THz,

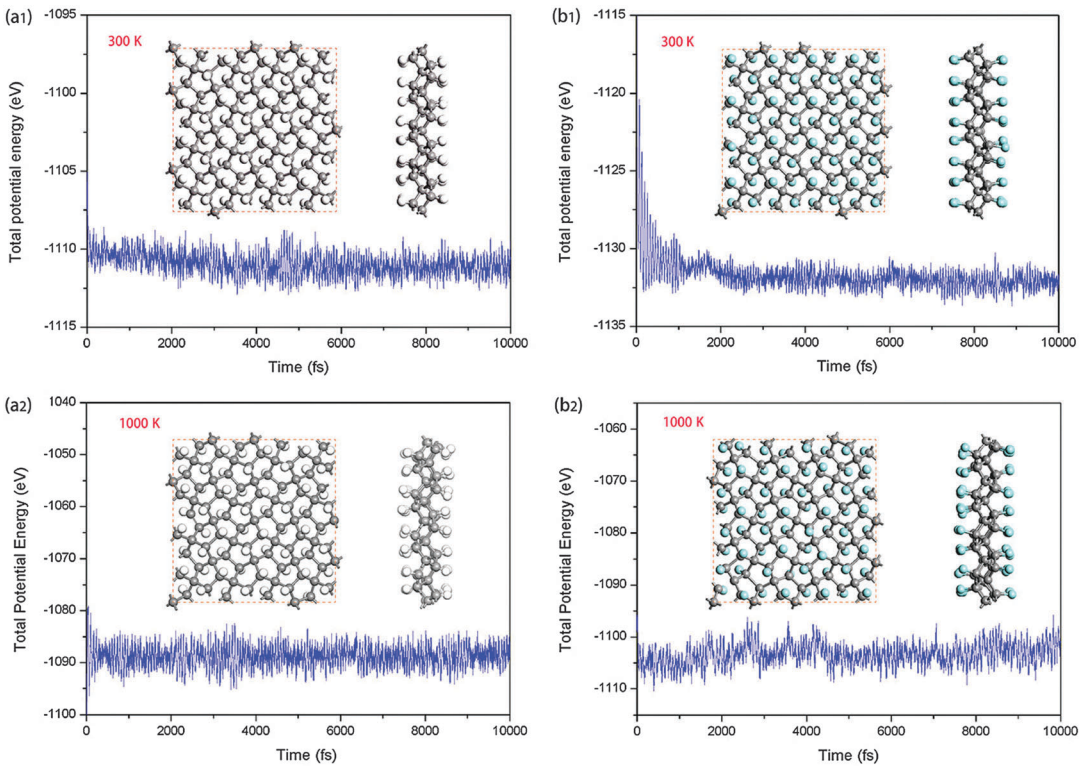

Fig. 2 The fluctuations of total potential energy of (a) H-PG-H and (b) F-PG-F during the AIMD simulations at 300 K and 1000 K. The insets are snapshots of the structures at the end of simulations.

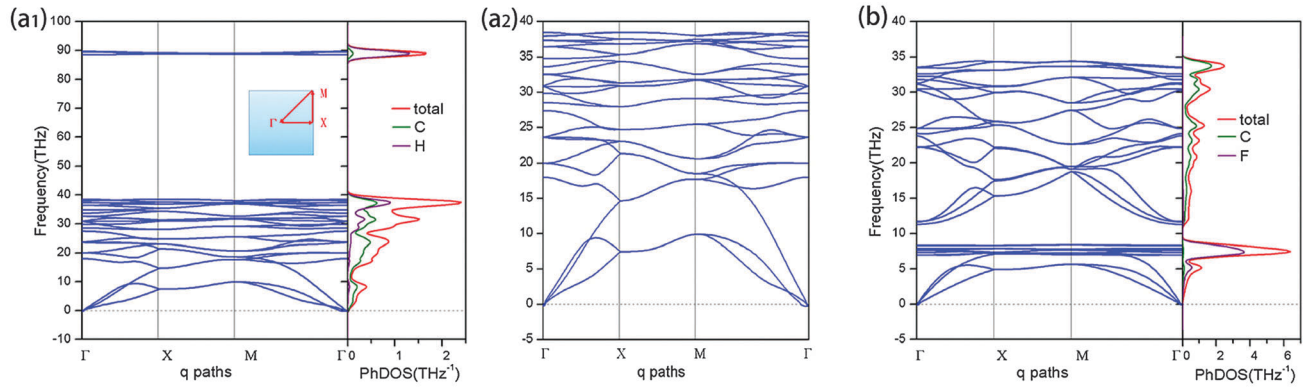

Fig. 3 Phonon band structures and corresponding atom-resolved PhDOS of (a_1) H-PG-H and (b) F-PG-F. (a_2) is the phonon band structures of H-PG-H in the low frequency region. The inset in (a_1) represents the high-symmetric q-point paths: Γ (0, 0)–X (1/2, 0)–M (1/2, 1/2)–Γ (0, 0).

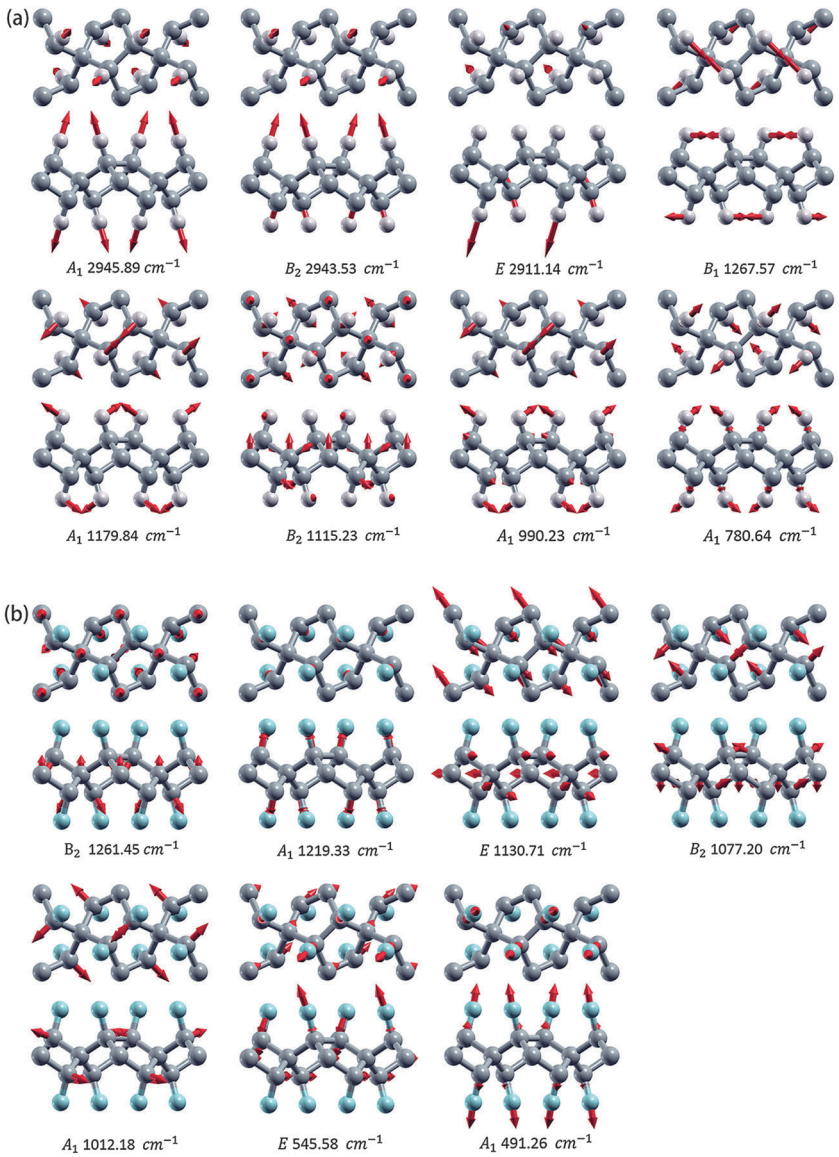

Fig. 4 Raman-active and IR-active modes of (a) H-PG-H and (b) F-PG-F. The degenerate modes are not shown here.

while the formation of C–H bonds and C–F bonds introduces several new vibration modes. Since the vibration frequency is inversely proportional to the effective mass and the atomic mass of fluorine is much bigger than that of the hydrogen atom, the vibration modes of C–H bonds mainly lie in the high frequency region which is much higher than that of double bonds of C2 atoms, whereas the phonon modes of C–F bonds are mainly located in the frequency range above acoustic modes.

We further analyzed the vibrational activity at the Γ point in the Brillouin zone center so that one can distinguish the hydrogenated and fluorinated penta-graphene by comparing their Raman and Infrared (IR) spectra. The hydrogenated and fluorinated penta-graphene both belong to the D_{2d} point group, and the irreducible representations of the phonons at the Brillouin zone center can be expressed as:

$$\Gamma = 4A_1(R) \oplus A_2 \oplus 3B_1(R) \oplus 4B_2(I + R) \oplus 8E(I + R)$$

where A_1 and B_1 modes are Raman-active, B_2 and E modes are both Raman- and infrared-active, and the A_2 mode is neither Raman-active nor infrared-active. Although there are same irreducible representations of phonons at the Γ point, the frequency and intensity of Raman/IR activity of vibration modes are different for the hydrogenated and fluorinated penta-graphene. In the case of H-PG-H, there is obvious Raman-activity at 2945.89, 2911.14, 1267.57, 1179.84, 1115.23, 990.23 and 780.64 cm^{-1}, IR-activity at 2943.53 and 2911.14 cm^{-1}, respectively. But for F-PG-F, the frequencies of pronounced Raman-active modes are 1219.33, 1077.20, 1012.18 and 491.26 cm^{-1} while the IR-active modes are 1261.45, 1130.71 and 545.58 cm^{-1}. The atomic vibration details of the Raman and IR active modes mentioned above are illustrated in Fig. 4.

To study the effect of the hydrogenation/fluorination on the electronic structure of penta-graphene, we calculated the electronic band structure and corresponding partial density of states (DOS) of the hydrogenated/fluorinated penta-graphene. The results are plotted in Fig. 5, which shows that H-PG-H/F-PG-F has an indirect band gap of 4.29 eV/3.36 eV at the PBE level. The underestimation of the PBE functional in predicting electronic

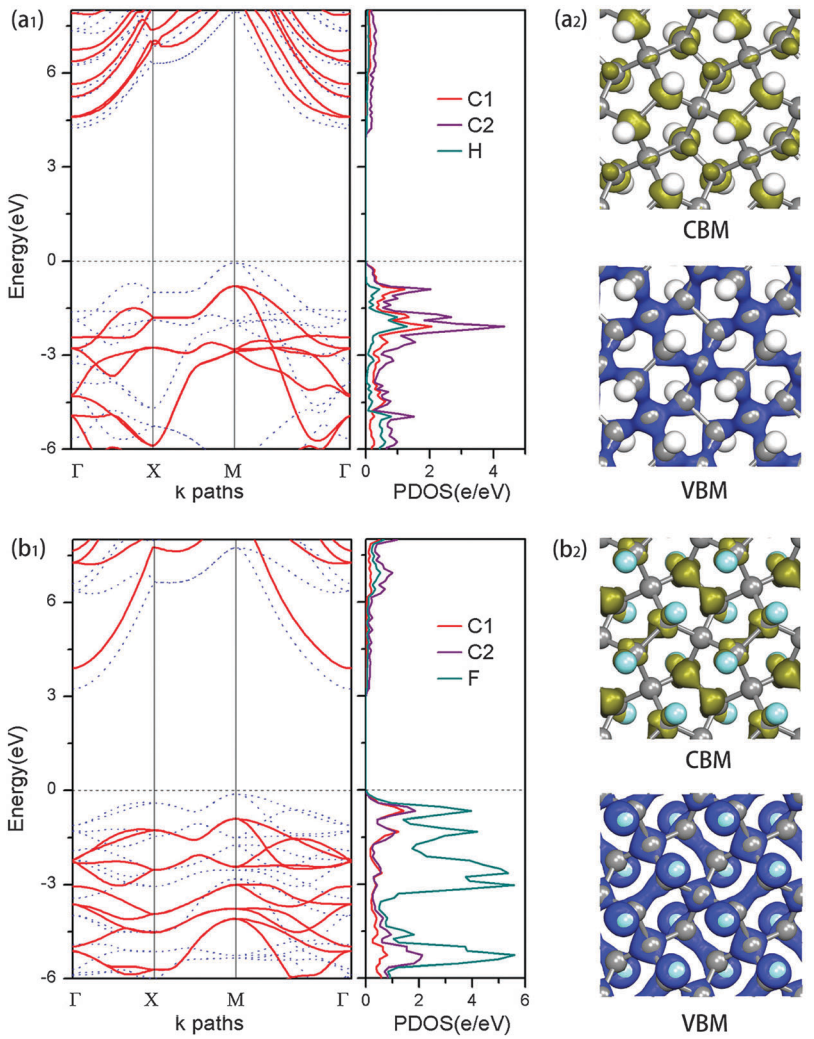

Fig. 5 Electronic band structure and atom-decomposed partial DOS of (a_1) H-PG-H and (b_1) F-PG-F. Blue dashed lines and red solid lines correspond to the PBE and HSE06 results, respectively. The corresponding band-decomposed charge density distributions of (a_2) H-PG-H and (b_2) F-PG-F.

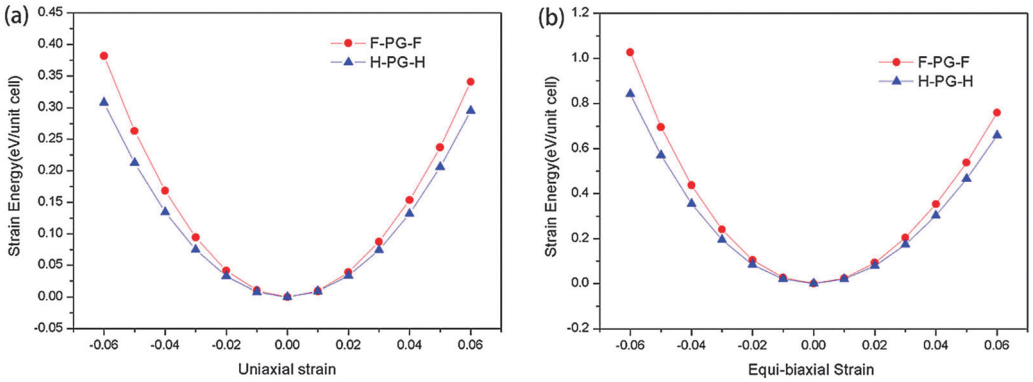

Fig. 6 Strain–energy relationship of the hydrogenated and fluorinated penta-graphene sheets under (a) uniaxial strain and (b) equi-biaxial strain.

band gaps of materials is well-known, and hence we used the hybrid HSE06 functional to get more accurate results. Although the band structures obtained by using the HSE06 functional are similar to those obtained by using the PBE functional, the band gaps change to 5.35 eV and 4.78 eV respectively, showing that both hydrogenation and fluorination can effectively tune the electronic structure of penta-graphene and change it from a semiconductor to an insulator. Thus, the functionalized penta-graphene sheets with low density and large band gap could serve as the dielectric layers in field effect transistors (FETs), substituting for silicon oxides.[29–31] The band gaps of graphane and fluorographene were calculated as well for comparison, and the results are presented in Table 1, in which the PBE results agree well with the previous studies.[32,33] Although the surface functionalized and pristine penta-graphene are all indirect band gap structures, as their valence band maximum (VBM) and conduction band minimum (CBM) are located at different k points in the momentum space: the VBM/CBM shifts from the Γ-X/M-Γ path to the M/Γ path respectively after the hydrogenation/fluorination, and the sub-VBM in penta-graphene disappears upon the functionalization, as shown in Fig. 5(a_1) and (b_1). This can be attributed to the redistribution of charge density. The charge density distributions of the band edge states for the hydrogenated and fluorinated penta-graphene were calculated and plotted in Fig. 5(a_2) and (b_2), respectively. The results show that the VBM state of the hydrogenated/fluorinated penta-graphene has σ_s and σ_{ps} characters while the CBM state has σ_s* and σ_{ps}* characters, which are different from that of penta-graphene. The atom-decomposed partial DOSs were calculated for further analysis of the electronic band structures. The partial DOS of the hydrogenated penta-graphene shows that the electronic states near the Fermi level are mainly from C1 and C2 atoms, while for the fluorinated penta-graphene, the partial DOS in the vicinity of the Fermi level originates from both of C and F atoms, which is confirmed by the band-decomposed charge density distributions (see Fig. 5). The difference of the partial DOS between the hydrogenated and fluorinated penta-graphene can be ascribed to the electronegativity of ad-atoms. The electronegativity increases from hydrogen to carbon to fluorine; therefore, in hydrogenated penta-graphene the C2 atoms serve as acceptors while in the fluorinated one they become donors, consistent with Bent's rule.[34,35] That is, in the case of H-PG-H the charge transfers from hydrogen to carbon while from carbon to fluorine for that of F-PG-F.

Table 2 Elastic constants, Young's modulus E, and Poisson's ratio ν of pristine and the functionalized penta-graphene

	PG[4]	H-PG-H	F-PG-F
C_{11} (GPa nm)	265	218.42	253.20
C_{12} (GPa nm)	−18	53.13	59.70
E (GPa nm)	263.8	205.50	239.12
ν	−0.068	0.243	0.236

Finally, we investigated the mechanical properties of the hydrogenated/fluorinated penta-graphene. Penta-graphene has robust mechanical stability and outstanding mechanical properties. How do they change upon hydrogenation and fluorination? To this end, we calculated the in-plane Young's modulus and Poisson's ratio of the hydrogenated and fluorinated penta-graphene by fitting the energy curves associated with uniaxial and equi-biaxial strains,[4] which are shown in Fig. 6. The calculated results are presented in Table 2. After surface modification, the in-plane Young's modulus for the hydrogenated and fluorinated penta-graphene is 205.50 and 239.12 GPa nm respectively, which is still comparable to 263.8 GPa nm of penta-graphene. The slight decrease of Young's modulus can be attributed to the difference in the bond order and bond type between pristine and the functionalized penta-graphene.

Conclusions

Motivated by the unique geometry and novel properties of penta-graphene proposed recently, and the advances of surface modification for 2D materials, we have studied the effect of hydrogenation and fluorination on the electronic and mechanical properties of penta-graphene. State-of-the-art theoretical calculations reveal that the surface-modified structures have higher thickness as compared to penta-graphene. The binding of hydrogen/fluorine atoms with penta-graphene is stronger than that with graphene. The functionalized sheets are not only dynamically and thermally stable at room temperature, but can also withstand temperatures as high as 1000 K. Hydrogenation and fluorination significantly widen the band gap of penta-graphene,

leading to the transformation from a semiconductor to an insulator. Compared with the fluorination, the hydrogenation results in a larger energy band gap, a larger Poisson's ratio but a smaller Young's modulus, and more Raman active modes with higher frequencies. The in-plane Young's modulus changes to 205.50/239.12 GPa nm from 263.8 GPa nm upon hydrogenation/fluorination. This study suggests that hydrogenation and fluorination can effectively tune the electronic and mechanical properties of penta-graphene for new potential applications.

Acknowledgements

This work was partially supported by grants from the National Natural Science Foundation of China (NSFC-51471004), the National Grand Fundamental Research 973 Program of China (Grant No. 2012CB921404), and the Doctoral Program of Higher Education of China (20130001110033). The computational resources for the present research were provided by the National Supercomputer Center in Guangzhou.

References

1 K. S. Novoselov, A. K. Geim, S. V. Morozov, D. Jiang, Y. Zhang, S. V. Dubonos, I. V. Grigorieva and A. A. Firsov, *Science*, 2004, **306**, 666–669.
2 D. S. L. Abergel, V. Apalkov, J. Berashevich, K. Ziegler and T. Chakraborty, *Adv. Phys.*, 2010, **59**, 261–482.
3 K. S. Novoselov, A. K. Geim, S. V. Morozov, D. Jiang, M. I. Katsnelson, I. V. Grigorieva, S. V. Dubonos and A. A. Firsov, *Nature*, 2005, **438**, 197–200.
4 S. Zhang, J. Zhou, Q. Wang, X. Chen, Y. Kawazoe and P. Jena, *Proc. Natl. Acad. Sci. U. S. A.*, 2015, **112**, 2372–2377.
5 W. Liu, M. S. Miao and J. Y. Liu, *RSC Adv.*, 2015, **5**, 70766–70771.
6 Z. Wang, X. F. Zhou, X. Zhang, Q. Zhu, H. Dong, M. Zhao and A. R. Oganov, *Nano Lett.*, 2015, **15**, 6182–6186.
7 M. Maruyama and S. Okada, *Jpn. J. Appl. Phys.*, 2014, **53**, 06JD02.
8 F. Karlicky, K. Kumara Ramanatha Datta, M. Otyepka and R. Zboril, *ACS Nano*, 2013, **7**, 6434–6464.
9 S. P. Lonkar, Y. S. Deshmukh and A. A. Abdala, *Nano Res.*, 2015, **8**, 1039–1074.
10 D. C. Elias, R. R. Nair, T. M. Mohiuddin, S. V. Morozov, P. Blake, M. P. Halsall, A. C. Ferrari, D. W. Boukhvalov, M. I. Katsnelson, A. K. Geim and K. S. Novoselov, *Science*, 2009, **323**, 610–613.
11 J. Zhou, Q. Wang, Q. Sun, X. S. Chen, Y. Kawazoe and P. Jena, *Nano Lett.*, 2009, **9**, 3867–3870.
12 J. Zhou, M. M. Wu, X. Zhou and Q. Sun, *Appl. Phys. Lett.*, 2009, **95**, 103108.
13 G. Kresse and J. Furthmuller, *Phys. Rev. B: Condens. Matter Mater. Phys.*, 1996, **54**, 11169–11186.
14 J. P. Perdew, K. Burke and M. Ernzerhof, *Phys. Rev. Lett.*, 1996, **77**, 3865–3868.
15 J. Heyd, G. E. Scuseria and M. Ernzerhof, *J. Chem. Phys.*, 2003, **118**, 8207–8215.
16 J. Heyd, G. E. Scuseria and M. Ernzerhof, *J. Chem. Phys.*, 2006, **124**, 219906.
17 H. J. Monkhorst and J. D. Pack, *Phys. Rev. B: Solid State*, 1976, **13**, 5188–5192.
18 S. Nose, *J. Chem. Phys.*, 1984, **81**, 511–519.
19 A. Togo, F. Oba and I. Tanaka, *Phys. Rev. B: Condens. Matter Mater. Phys.*, 2008, **78**, 134106.
20 J. O. Sofo, A. S. Chaudhari and G. D. Barber, *Phys. Rev. B: Condens. Matter Mater. Phys.*, 2007, **75**, 153401.
21 H. Prinzbach, A. Weiler, P. Landenberger, F. Wahl, J. Worth, L. T. Scott, M. Gelmont, D. Olevano and B. V. Issendorff, *Nature*, 2000, **407**, 60–63.
22 E. Sackers, T. Osswald, K. Weber, M. Keller, D. Hunkler, J. Worth, L. Knothe and H. Prinzbach, *Chem. – Eur. J.*, 2006, **12**, 6242–6254.
23 P. V. Medeiros, A. J. Mascarenhas, F. de Brito Mota and C. M. de Castilho, *Nanotechnology*, 2010, **21**, 485701.
24 D. Yi, L. Yang, S. J. Xie and A. Saxena, *RSC Adv.*, 2015, **5**, 20617–20622.
25 C. A. Marianetti and H. G. Yevick, *Phys. Rev. Lett.*, 2010, **105**, 245502.
26 C. Si, W. Duan, Z. Liu and F. Liu, *Phys. Rev. Lett.*, 2012, **109**, 226802.
27 N. Sheppard, *J. Chem. Phys.*, 1949, **17**, 74.
28 S. Sakong and P. Kratzer, *J. Chem. Phys.*, 2010, **133**, 054505.
29 S. Shaikhutdinov and H. J. Freund, *Adv. Mater.*, 2013, **25**, 49–67.
30 T. Hattori, K. Takahashi, M. B. Seman, H. Nohira, K. Hirose, N. Kamakura, Y. Takata, S. Shin and K. Kobayashi, *Appl. Surf. Sci.*, 2003, **212**, 547–555.
31 G. D. Wilk, R. M. Wallace and J. M. Anthony, *J. Appl. Phys.*, 2001, **89**, 5243.
32 O. Leenaerts, H. Peelaers, A. D. Hernandez-Nieves, B. Partoens and F. M. Peeters, *Phys. Rev. B: Condens. Matter Mater. Phys.*, 2010, **82**, 195436.
33 M. Klintenberg, S. Lebegue, M. I. Katsnelson and O. Eriksson, *Phys. Rev. B: Condens. Matter Mater. Phys.*, 2010, **81**, 085433.
34 H. A. Bent, *Chem. Rev.*, 1961, **61**, 275–311.
35 D. M. Lemal, *J. Org. Chem.*, 2004, **69**, 1–11.